A Three-Dimensional Simulation of the Hudson–Raritan Estuary. Part II: Comparison with Observation

LIE-YAUW OEY* AND GEORGE L. MELLOR

Geophysical Fluid Dynamics Program, James Forrestal Campus, Princeton University, Princeton, NJ 08542

RICHARD I. HIRES

Department of Civil & Ocean Engineering, Stevens Institute of Technology, Hoboken, NJ 07030

(Manuscript received 12 December 1984, in final form 31 May 1985)

ABSTRACT

Results from a time-dependent, three-dimensional numerical simulation of the Hudson–Raritan estuary are compared with observations. The comparison includes: 1) instantaneous salinity contours across a transect in the estuary; 2) amplitudes and phases of tidal constituents at four tide gauge and five current meter stations; 3) mean currents at nine meter locations, and mean salinity in the Hudson River; 4) kinetic energy spectra; and 5) response to wind forcing of subtidal current at an observational station near the mouth of the estuary.

Observations confirm the model's prediction of existence of density advection instabilities induced by differential advection of the three-dimensional density field. These instabilities produce intense vertical mixing and should significantly modify dispersion processes in the estuary. Effects of neap–spring tides on vertical stratifications are also simulated by the model. Simulated M_2 phases at three tide gauge stations show improvement over the M_2 phases obtained from a two-dimensional, vertically integrated tidal model. The improvement is presumably due to bottom boundary layer resolution and, therefore, improved representation of bottom friction in the three-dimensional model. Simulated (instantaneous and mean) currents compare reasonably well with observations, except at narrow channel regions where the model's resolution is inadequate. Simulated "density-induced" mean currents are weaker than those observed, a discrepancy attributed to neglect of temperature variations in the model. Horizontal diffusion coefficients are null in this model. The burden of horizontal dispersion is generally handled well by the model's adequate resolution of small-scale advective processes, as suggested by the model's correct simulation of the k^{-3} transfer spectrum law at high wavenumber k. In narrow rivers that are modeled two-dimensionally (x, z), the estimate of the horizontal dispersion due to vertical variabilities in velocity and salinity appears to be correct; however, mixing by lateral variability is absent so that the saline intrusion is somewhat underpredicted. At the mouth of the estuary, simulated subtidal current responses to wind forcing generally agree with observed responses. The response is partly barotropic, which is a result of balance between bottom friction, sea level setup from the adjacent continental shelf and wind stress, modified by local vertical velocity shears and baroclinic responses.

1. Introduction

In Part I (Oey *et al.*, 1985a), we discussed numerical results obtained from a 216-day simulation of the Hudson–Raritan estuary. In Part II, we compare numerical results with observations made during August 1980 by the National Ocean Survey (NOS). To experimentally verify density advection instabilities elucidated in Part I, we shall also compare the computed salinity distribution across the Sandy Hook–Rockaway Point transect (henceforth the SHRP transect) with our own field data.

The NOS circulatory study consisted of six 15-day deployment periods of current meters during summer and fall of 1980. For the present study, NOS current meter observations from the first two deployment periods (4 August 1980–3 September 1980) were used. There were nine stations in the first deployment period and ten in the second. Observations from some of these stations were rejected owing either to meter malfunction or to unrealistically large values of velocity. For the present study we decided to use the current meters from the SHRP transect, the Narrows and the Hudson River. These are regions of largest tidal current amplitudes in the harbor and are also regions where most of the tidal energy is produced and dissipated. The locations of the current meter stations are shown in Fig. 1. Further information on these observations is provided in Table 1. We have retained the NOS station numbers but have added suffixes *S*, *M* or *B* to denote the near-surface, middle and near-bottom meters.

The current meters used in the NOS study were Grundy Model 9021-G meters which measure temperature and conductivity together with current speed and direction. The sampling interval was ten minutes. Initial processing of the current meter records was per-

* Present Affiliation: Skidaway Institute of Oceanography, Post Office Box 13687, Savannah, GA 31416.

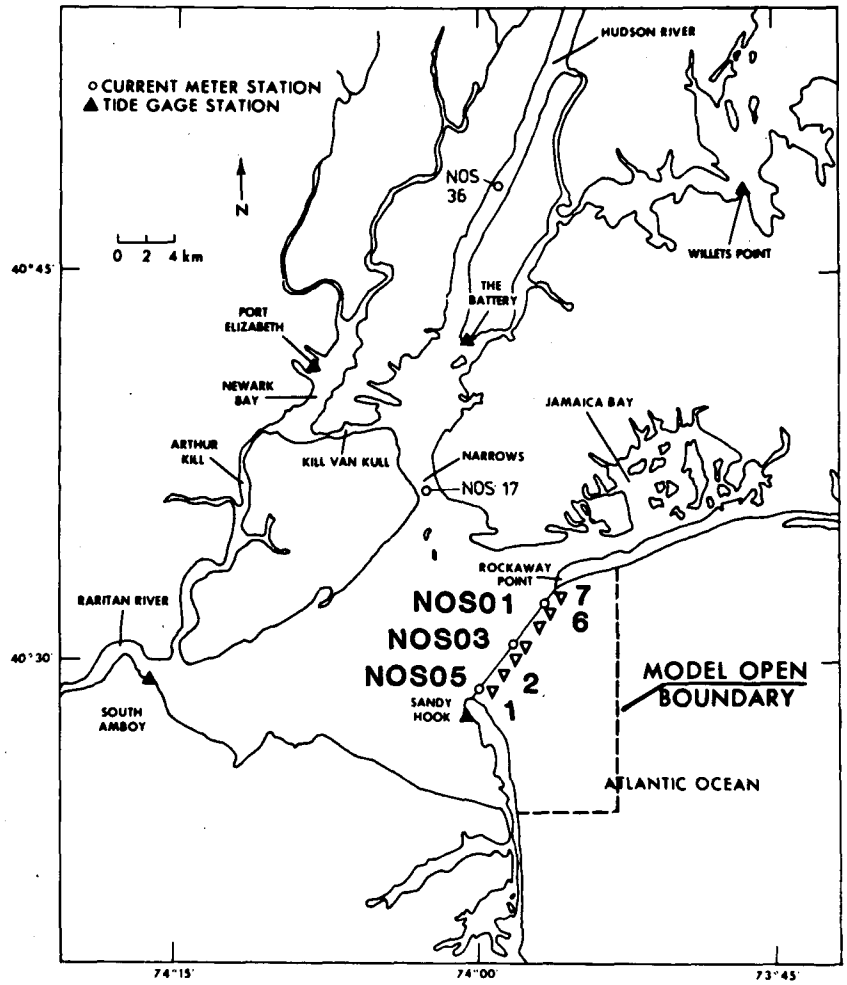

FIG. 1. Locator map of the Hudson–Raritan estuary, showing tide gauge stations and NOS current meter locations where computed tides, velocity and salinity are compared with observations. The triangular symbols across the Sandy Hook–Rockaway Point transect denote stations where salinity measurements were taken on 20 and 27 August 1980.

formed by NOS. Copies of the processed data files were made available to us by NOS. Further details on instrumentation as well as a discussion of measurement uncertainty for these instruments are given by Kalvaitis (1982).

There are three reference tide gauge stations in the New York Harbor region: Sandy Hook, the Battery and Willets Point. During the NOS circulatory study several supplementary gauges were installed. In addition to sea level elevation data from these reference stations we have also employed data from tide gauges at South Amboy near the Raritan River mouth and at Port Elizabeth in Newark Bay.

2. Experimental verification of density advection instabilities

In Part I, we discussed a new mechanism for intense mixing produced by dense water overlying less dense water owing to differential advection of the three-dimensional salinity field by tidal and/or wind-induced currents. We called this phenomenon a density advection instability and cited field measurements by Bowden *et al.* (1959) that indirectly suggest existence of such instabilities. We now present our own observed salinity (density) variations across the SHRP transect and compare these "synoptic" observations with simulated results. Our objective is to show that unstable layers of water do develop in the estuary.

a. Observational procedure

Temperature and conductivity measurements were taken on a small boat using a Beckman RS-5 salinometer at seven more or less evenly spaced stations along the SHRP transect (Fig. 1). The vertical (z-direction) spacing at each station was approximately 1.6 m with the first meter reading taken at 1.6 m below the water

TABLE 1. NOS meter locations.

Station	Meter depth (m)	Location Latitude (°N)	Location Longitude (°W)	Water depth (m)	Record duration Month/day/GMT-Month/day
NOS 01		40 82 18	73 56 48	7.9	
S	5.2				08/04/1500-08/21
B	6.7				08/15-09/05
NOS 03		40 30 54	73 58 24	13.4	
S	5.5				08/04/1700-08/21
NOS 03		40 30 48	73 58 18	13.4	
S	5.5				08/21-09/04
B	12.2				08/29-09/01
NOS 05		40 29 12	74 00 06	14.0	
S	4.6				08/04/1800-09/02
B	12.8				08/13/0600-09/04
NOS 17		40 36 30	74 02 54	25.9	
S	3.0				08/06/2200-08/20
M	17.1				08/23/1500-09/05
B	24.7				08/20/1700-09/05
NOS 36		40 48 48	73 58 06	16.2	
S	4.9				08/20/1600-09/04

surface. Measurements were repeated at about 1.5-hour intervals at each station over a tidal cycle on 6, 20 and 27 August 1980.

b. Comparison of salinity distributions

In order to compare observed and computed salinity distributions at a particular instant of time, a linear, time interpolation of observed values at each observation point was used. This and the fact that the measurement stations were not aligned exactly along a straight line across the SHRP transect introduce possible sources of discrepancy in the comparison. We shall present results for the 20 and 27 August periods which represent respectively a neap and a spring tide sample. Thus the effect of different tidal amplitudes on stratification can also be seen.

Figures 2a, b show comparisons of computed and observed salinity contours at approximately slack before flood (1500 GMT 20 August and 2100 GMT 27 August). The model simulates fairly well the observed salinity features in the midsection (Fig. 2a), except that it misses the high bottom salinity value ($S \approx 32‰$). The model also misses the observed pool of near-surface, rather fresh water ($S \approx 28$–$28.5‰$) close to Sandy Hook. This is due to neglect of the Shrewsbury River discharge just south of Sandy Hook on the southern portion of the model boundary. Its total discharge amounts to only 5% of the discharge from Raritan River, but its close proximity exerts a significant local influence. Between the midsection and Rockaway Point, the simulation shows a near-surface, rather fresh pool of water ($S \approx 29.5‰$, Fig. 2a) that is due to sewage discharge from Jamaica Bay. The observed salinity does not show this feature. One notes however that this pool of surface water was simulated to occur at a depth of less than 2 meters below mean tide level and could therefore be missed by the coarse vertical resolution used in the observations. Nevertheless, the observed near-surface (<2 m) salinity at station 7 is less than that at station 6, which suggests that there is less saline water close to the Rockaway Peninsula shoreline flowing out from Jamaica Bay during the previous ebb cycle.

Figure 2a also shows unstable stratifications in the observed salinity contours. Vertical difference in salinity (upper salinity minus lower salinity) is +0.14‰ near Sandy Hook, and surface and bottom vertical salinity differences are +0.11‰ and +0.18‰, respectively, near Rockaway Point. The precision of salinity measurements is within ±0.02‰ so that differences greater than ±0.02‰ in observed salinities are considered significant. Observed density fields also show these instabilities, so these are true instabilities in the sense discussed in Part I and would produce intense vertical mixing. Simulation shows the instabilities near Rockaway Point but misses the one near Sandy Hook.

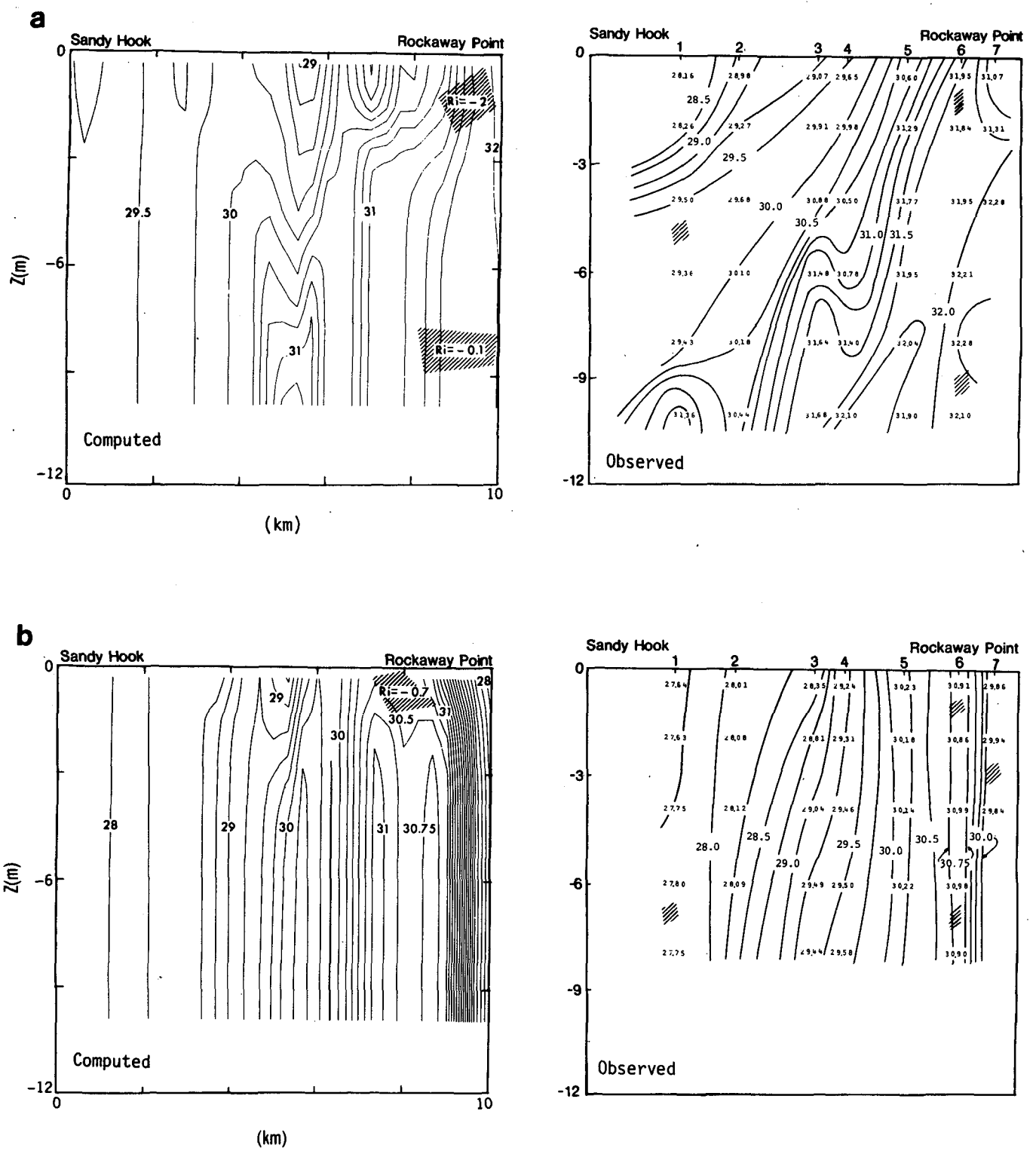

FIG. 2. Comparison of computed (left panel) and observed salinity (ppt) distributions across the Sandy Hook–Rockaway Point transect. The hatched areas are where the water columns are unstably stratified. The computed gradient Richardson numbers Ri are also shown. (a) 1500 GMT 20 August; (b) 2100 GMT 27 August; (c) 2000 GMT 20 August; (d) 1500 GMT 27 August. (a) and (b) correspond approximately to pre-flood slack and (c) and (d) to pre-ebb slack. The small numbers on the observed plots are salinity values in ppt at meter locations.

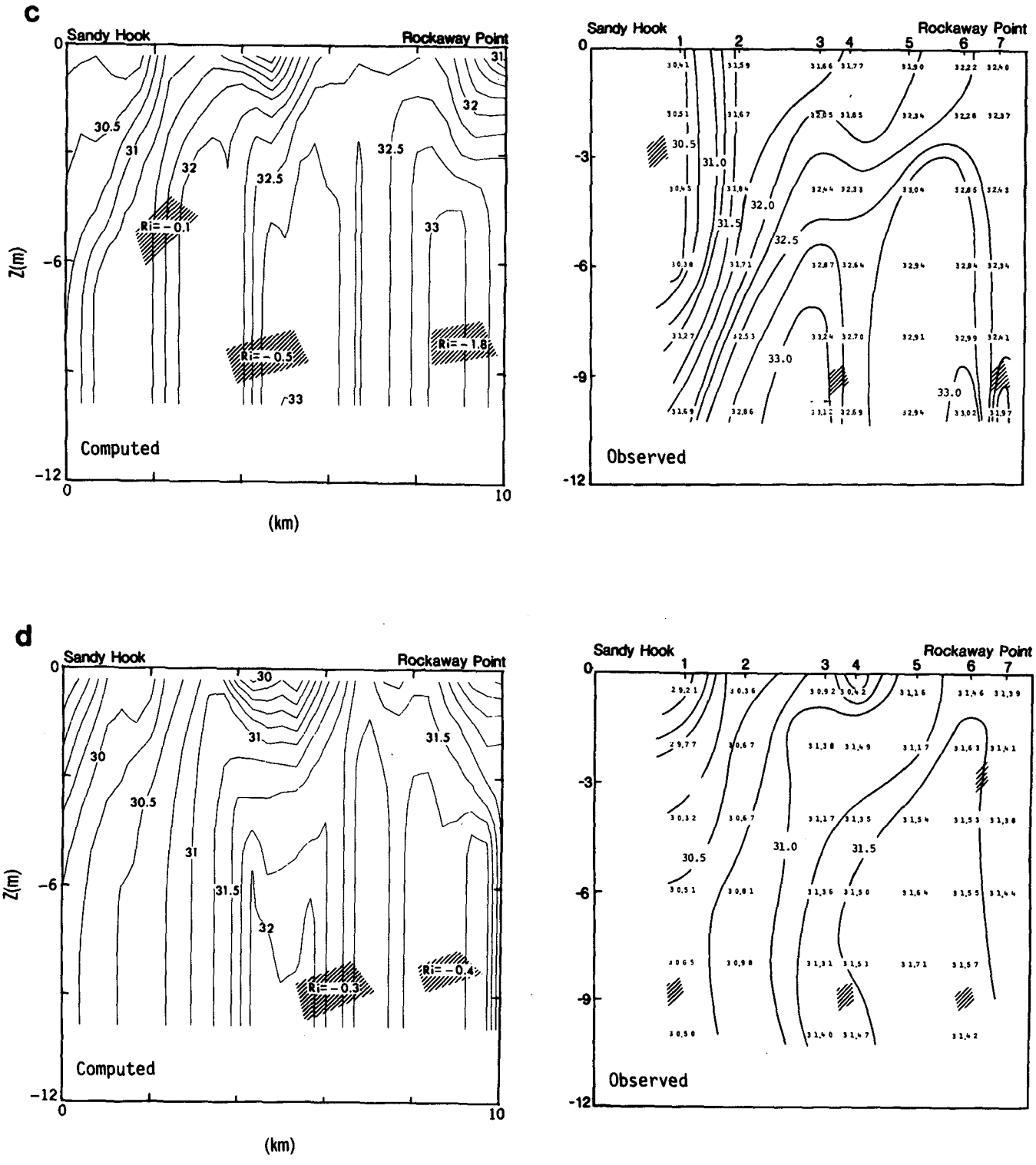

FIG. 2. (*Continued*)

Observed slack-before-flood salinity distributions during a spring tide (Fig. 2b) show vertically homogeneous water. The simulation also shows this feature as well as the observed unstable stratification in near-surface water close to Rockaway Point but misses the ones at 3 and 7 m and a similar one at 7 m near Sandy

Hook. The simulation shows a thin vertical column of rather freshwater ($S \approx 29.0‰$) close to Rockaway Point, which is also observed, although observation does not show such low salinity. There is also less-saline water close to Sandy Hook, which is again missed by the model. Excluding these thin columns of less-saline water, the transverse salinity difference is simulated well by the model.

Figures 2c, d compare computed and observed salinities at approximately slack before ebb (2000 GMT 20 August and 1500 GMT 27 August). The simulation shows formation of the near-surface salinity minimum and middepth stratification at the midsection but misses a deeper stratification (Fig. 2c). Locations of unstable stratifications are simulated well by the model as are the transverse and vertical differences of salinity. Observations do not show the rather fresh, near-surface water near Rockaway Point, however.

Finally, in Fig. 2d, the near-surface salinity minimum at the midsection and locations of unstable stratifications near Rockaway Point and at the midsection are simulated well, but those near the surface near Rockaway Point and one at 9 m depth near Sandy Hook are not simulated. The observed salinity at station 7 is again less than that at station 6. This feature is also simulated by the model, although the model salinity is lower than that observed (model salinity = 30.5‰; observed salinity = 31.40‰). Transverse and vertical salinity differences are also simulated well by the model.

It appears that the model simulated quite well the observed salinity distributions across the transect. Discrepancies in local regions can largely be explained by errors we made in specifying freshwater discharges from small streams and sewage sources. The model also predicts weaker stratifications in the Ambrose Channel at the midsection of the transect. This is most likely due to neglect of temperature in the model and we shall discuss this in more detail after examining the NOS data. The model's prediction of unstable stratifications is confirmed by observations. Temporal durations of density advection instabilities ($Ri < 0$) in the model calculation are about 1–2 hours and are marginal when comparing with observations with time resolution of about 1.5 hours. Thus we can only verify the existence of these instabilities and should not be overly concerned with the model's failure to reproduce them exactly in time and space.

3. Comparison of model results with NOS observations

We first compare model and observational results at both the tidal time scales of one day and less, and at the subtidal time scales of one to ten day periods. In addition to customary time series comparisons we also compare the spectral distributions between the observed and simulated currents. This enables us to compare simulated and observed responses to subtidal wind forcings. These comparisons in Fourier space provide additional demonstration of model skill (cf. Bedford, 1981).

a. Comparison of tidal elevations

Figure 3 gives an example of comparison of computed and observed tides at the Battery from 3 August through 2 September 1980. Computed amplitude is a little low, while the phase generally agrees with observations. A summary of tidal harmonic analyses of the five major constituents for the four tide gauge stations shown in Fig. 1 is given in Table 2. Agreements between computed and observed amplitudes are best for M_2 and N_2 components. Excluding the Port Elizabeth tide station, computed M_2 amplitudes and phases are within 5% of observations. Tides from the SHRP transect to the Battery appear as progressive waves, and the good simulation suggests that the model has computed bottom friction well. Computed phases are improved over those obtained from a depth-averaged model with quadratic bottom friction and constant friction coefficient k ($\approx 2.5 \times 10^{-3}$), given by Oey *et al.* (1985c) and shown also in Table 2. A large part of the discrepancy in the two-dimensional model is due to uncertainties in the value of k. The model's resolution is poor, and amplitude and phase errors are large at Port Elizabeth, Newark Bay, which is connected to the main bay via narrow straits and which has narrow ship channels.

b. Comparison of velocity and salinity at the tidal time scales

Figure 4 shows examples of time series comparison between model results and observations. Here, longitudinal velocity at a particular station is defined as the velocity component normal to the local cross-sectional plane that passes through the station and is bounded on two sides by local coastline. In general, the model gives better simulation (Fig. 4a) during a spring tide (around 28 August) than during a neap tide (around 17 August). This happens because the model generally also computes less stratification than that which is observed, perhaps a consequence of the neglect of temperature variation in the simulation.

The model simulation at NOS36 (Fig. 4d) in the Hudson River is good, suggesting that the saline intrusion into the river has been simulated well. Figure 5 shows the simulated (solid curve) 30-day time-averaged and cross-sectionally averaged salinity distribution in the Hudson River. The dashed curve is from observations compiled by Quirk *et al.* (1971) for a different discharge and is included here to show that the model has computed well the shape of the longitudinal salinity variation in the river, including a slow, approximately linear rise of salinity with distance from the head of

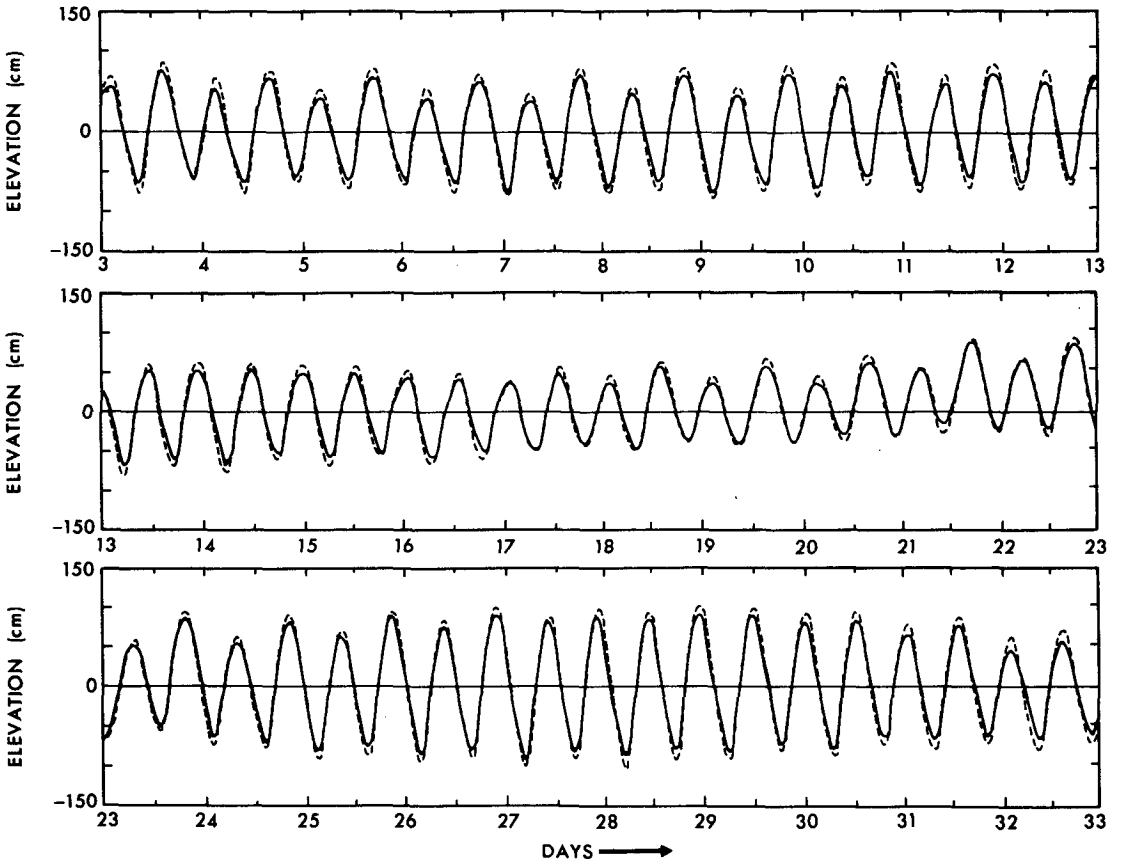

FIG. 3. Comparison of 30-day tide at the Battery from 3 August to 2 September. Solid curves are model results and dashed curves are observations.

the river, and a subsequent exponential variation further seaward. Quirk *et al.* reported an observed intrusion of about 120 km for a discharge of 130 $m^3 s^{-1}$ ($\approx$ mean discharge during simulation period) so that the computed salinity intrusion ($\approx$93 km) is smaller than that observed by about 23%. Since the model's

TABLE 2. Comparison of model (M) and observed (O) tidal elevation constituents at four tide gauge stations in New York Harbor. The bracketed numbers under the "M_2" column are computed phases obtained from Oey *et al.* (1985c) with a vertically integrated tidal model forced by an M_2 tide at the open boundaries.

	Constituents									
	M_2 tide		N_2		S_2		K_1		O_1	
Station	Amplitude (cm)	Phase (deg)	Amplitude (cm)	Phase (deg)	Amplitude (cm)	Phase (deg)	Amplitude (cm)	Phase (deg)	Amplitude (cm)	Phase (deg)
Sandy Hook										
M:	65.1,	23	15.0,	38	12.0,	267	9.8,	266	4.8,	117
O:	67.9,	23	14.8,	35	12.9,	260	9.9,	266	5.6,	114
South Amboy										
M:	71.1,	26 (28)	17.4,	38	12.1,	267	10.5,	266	5.2,	117
O:	74.8,	26	17.2,	39	14.9,	264	9.5,	266	5.3,	113
The Battery										
M:	67.8,	44.3 (50)	16.4,	64	11.8,	279	10.0,	275	4.9,	129
O:	68.6,	43.4	14.9,	59	12.3,	274	8.8,	279	6.8,	130
Port Elizabeth										
M:	67.2,	46.6 (45.7)	16.4,	65	12.7,	283	10.1,	268	4.9,	133
O:	77.5,	47.9	16.3,	63	14.1,	287	10.2,	282	6.7,	130

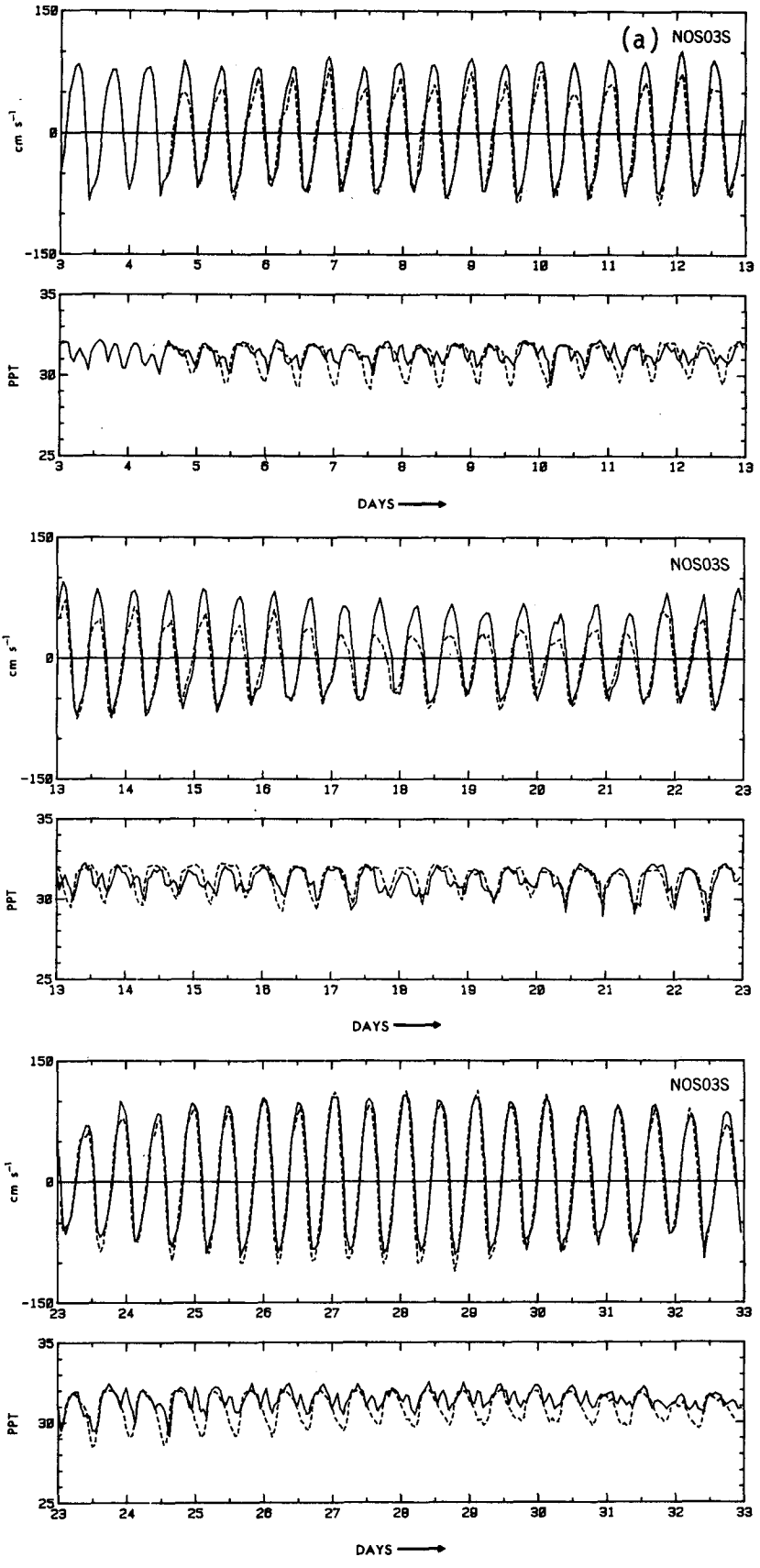

FIG. 4. Comparisons of time series of longitudinal velocity and salinity at NOS stations: (a) 03*S*, (b) 05*S*, (c) 17*M* and (d) 36*S*. Solid curves are model results and dashed curves are observations.

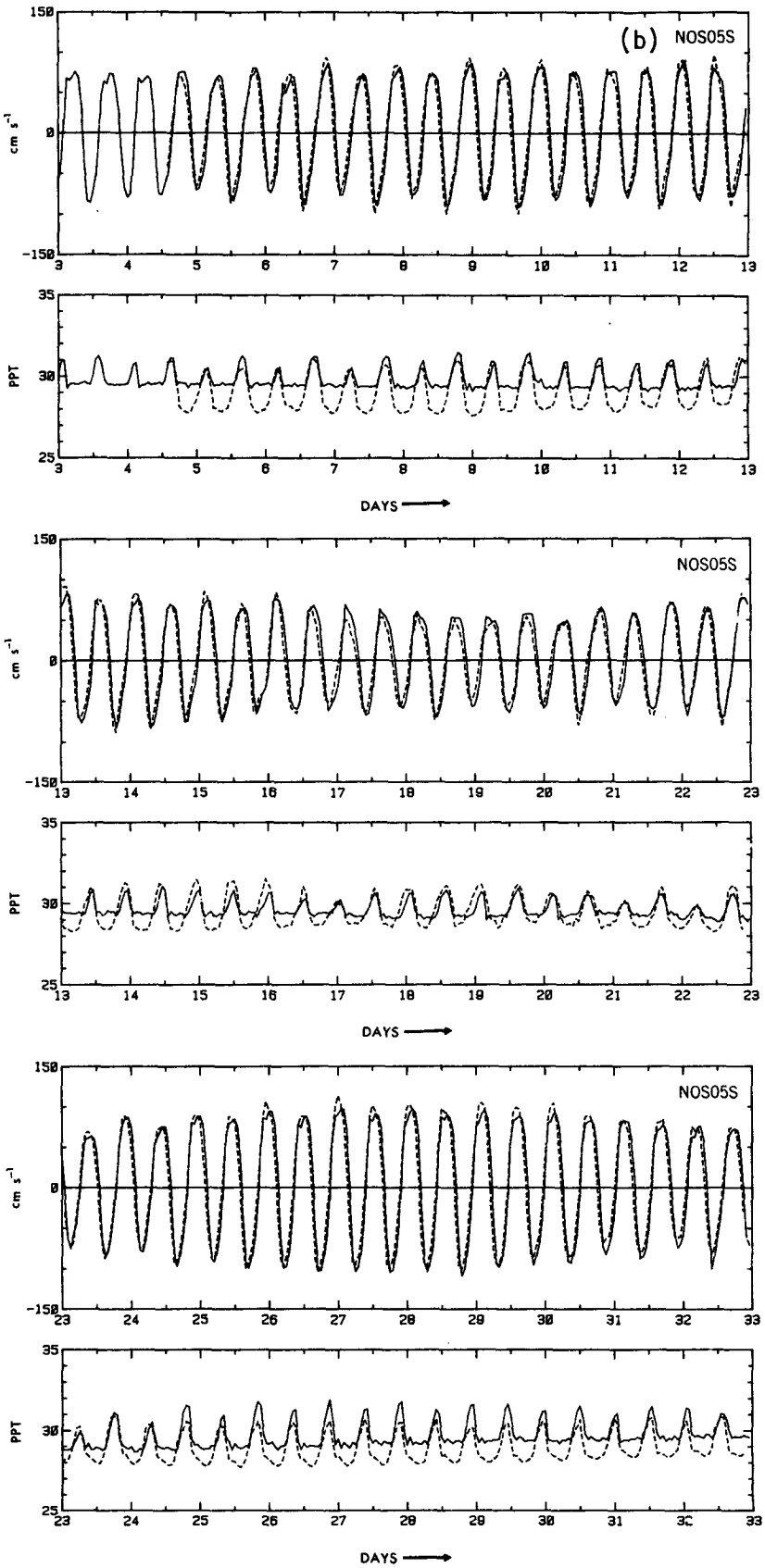

FIG. 4. (*Continued*)

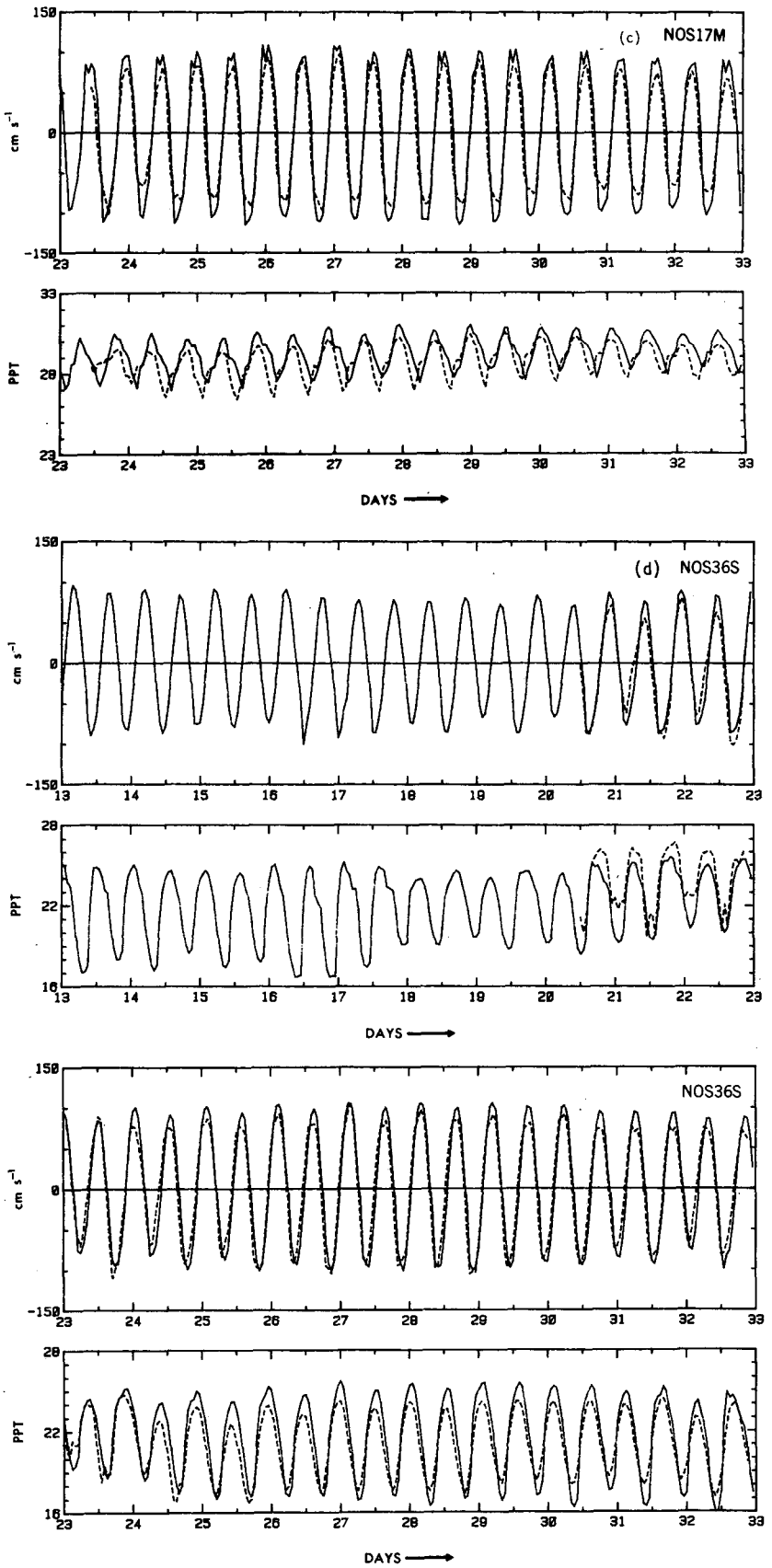

FIG. 4. (*Continued*)

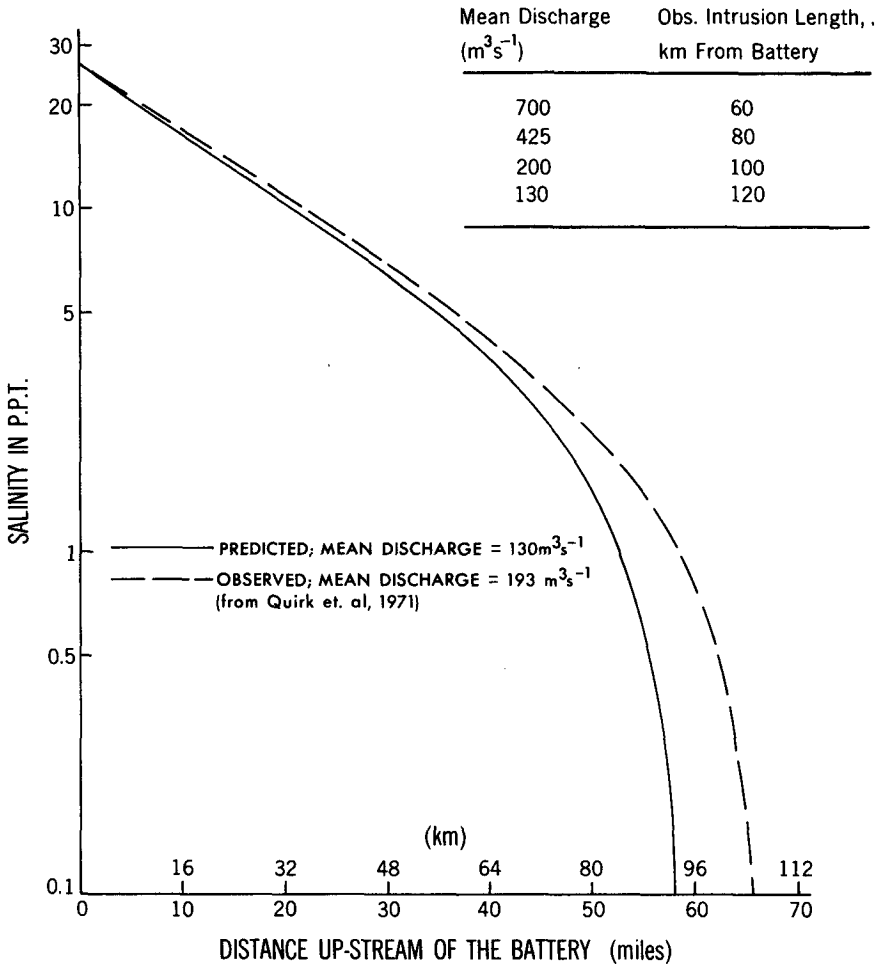

FIG. 5. A comparison of simulated (solid curve) and observed (dashed curve) time averaged and sectionally averaged salinity distribution in the Hudson River. Observations are taken from Quirk *et al.* (1971). Note that the log–linear plot exaggerates the difference between the computed and observed results at low salinity values.

horizontal diffusion has been set to zero, this deficiency in salt intrusion—if it is assumed that results of Quirk *et al.* apply to August 1980—may be a result of processes that are not included in the model, namely, the steady and unsteady transverse (across-river) variations of velocity and salinity. This is consistent with both observational evidence and analytical calculation, which give values of 55–80% for the fraction of upriver salt transport by the steady and unsteady vertical variations of velocity and salinity (see Oey, 1984, and references quoted therein). This implies that the model's vertical grid resolution (10 levels in depth of about 10 m) is sufficient to simulate dispersion processes induced by vertical velocity and salinity variations.

Results at NOS05 (Fig. 4b) illustrate well the effects on salinity variations of eddies produced by interaction between tidal currents and coastal promontories. Seawater that passes NOS05 during a flood is trapped and mixed in Sandy Hook Bay with less-saline water from the Raritan and Shrewsbury rivers. This process is carried out by eddies generated by the interaction of flooding currents with Sandy Hook Peninsula (Fig. 4, Part I). During ebb, water of almost constant salinity stored in Sandy Hook Bay now flows out and passes station NOS05 resulting in a "flat" salinity trough as shown in Fig. 4b. This asymmetry in salinity variation is simulated quite well by the model, except that observed salinities during ebb (the "flat trough") are on average 0.8‰ lower. This discrepancy is in part caused by freshwater discharge from the Shrewsbury River (Fig. 1, Part I), which we thought to be unimportant and therefore neglected in the model. Its close proximity to NOS05 apparently has a significant, local influence on the salinity and, as we shall see later, on density-induced mean flow also.

We summarize in Table 3 results of velocity comparison in terms of harmonic constituents. Largest discrepancies are at the Narrows (see also Fig. 4c) where the model overpredicts the observed velocity magnitude at NOS17*S* by as much as 50% during neap tides

TABLE 3. Comparison of model (M) and observed (O) tidal-current constituents in New York Harbor. See Table 1 for meter depths.

	Tidal constituents (period in hours)													
	M_2 (12.4206)		N_2 (12.6583)		S_2 (12.000)		K_1 (23.9345)		O_1 (25.8193)		M_4 (6.2103)		M_6 (4.1402)	
NOS station	Amplitude (cm s^{-1})	Phase (deg)	Amplitude (cm s^{-1})	Phase (deg)	Amplitude (cm s^{-1})	Phase (deg)	Amplitude (cm s^{-1})	Phase (deg)	Amplitude (cm s^{-1})	Phase (deg)	Amplitude (cm s^{-1})	Phase (deg)	Amplitude (cm s^{-1})	Phase (deg)
01S														
M:	64.5,	128.9	15.0,	141.6	13.1,	10.0	4.8,	2.5	2.6,	233.1	3.5,	85.4	7.5,	265.2
O:	79.6,	114.8	19.3,	129.9	15.2,	−3.4	6.2,	4.7	1.8,	230.0	6.5,	63.4	6.3,	226.8
03S														
M:	76.5,	154.7	15.1,	164.0	13.4,	25.2	4.6,	7.6	3.2,	221.0	8.4,	40.0	5.9,	314.4
O:	66.2,	148.9	19.1,	166.2	15.1,	24.4	6.9,	23.0	2.7,	225.0	9.6,	63.1	5.2,	274.2
05S														
M:	80.9,	147.8	15.0,	158.0	13.5,	17.0	5.1,	14.0	3.1,	210.0	9.3,	83.6	8.8,	290.3
O:	78.0,	140.5	14.7,	150.8	14.7,	7.6	6.2,	20.0	2.9,	235.0	7.2,	28.4	4.9,	282.4
05B														
M:	43.0,	148.3	7.8,	151.3	7.4,	26.3	2.8,	13.0	1.3,	203.7	3.2,	41.5	2.4,	257.6
O:	43.8,	148.1	20.8,	140.6	15.7,	−4.7	4.0,	19.0	1.7,	165.1	5.5,	−5.0	1.8,	219.9
17S														
M:	115.1,	186.6	20.6,	14.0	14.4,	−3.6	4.2,	44.1	3.5,	260.8	9.6,	198.0	3.3,	53.6
O:	82.6,	188.4	13.5,	12.4	12.7,	53.0	7.9,	54.0	3.5,	253.4	4.7,	87.0	2.1,	51.4
17M														
M:	84.9,	175.2	16.9,	169.8	11.3,	12.3	5.1,	18.2	5.7,	234.0	9.9,	112.3	11.8,	352.1
O:	69.8,	174.8	16.9,	192.0	12.5,	36.0	6.6,	55.0	4.8,	264.0	7.6,	22.0	9.5,	303.1
17B														
M:	59.2,	174.5	10.8,	180.0	6.4,	28.8	2.2,	15.0	2.6,	218.2	3.5,	85.0	5.2,	342.7
O:	52.1,	171.0	14.6,	195.0	10.4,	47.0	5.8,	63.0	4.0,	278.0	4.4,	351.0	8.0,	288.0
36S														
M:	84.7,	223.2	13.4,	254.0	7.1,	92.3	8.5,	60.5	4.5,	264.4	2.1,	176.0	2.0,	190.3
O:	85.0,	218.3	14.1,	248.0	11.4,	81.4	14.2,	81.0	10.7,	284.0	6.6,	117.2	4.7,	141.0

(not shown). The error may again be due to neglect in the model calculation of temperature variation, which is expected to be important at the Narrows because of its greater depth and dynamically more significant during neap period when tidal mixing is weak.

c. *Comparison of mean velocities*

We compare in Table 4 simulated and observed mean currents. The table also includes current meter data across the SHRP transect obtained from U.S. Coast and Geodetic Survey field studies for 12–16 August 1959, as reported by Doyle and Wilson (1978). The Hudson River discharge for August 1959 was 148 $m^3 s^{-1}$ and is therefore close to the present mean value of 130 $m^3 s^{-1}$. The largest discrepancy between simulation and observations occurs at NOS05 where both NOS and Doyle and Wilson observations give landward inflows in the deep Sandy Hook Channel (NOS05*B*), whereas the model's mean currents are seaward throughout the depth. This error is related to the model's poor prediction of salinity during ebb at NOS05 (Fig. 4b) and is in part due to neglect in the model calculation of a freshwater source from Shrewsbury River. Model grid sizes are also too coarse to resolve the narrow channel (width < 300 m). Apart from this localized error, overall agreement is fairly good. Both model and observations give landward flows near Rockaway Point (NOS01), surface seaward flows at midsection (NOS03*S*) and also near Sandy Hook (NOS05*S*), and weak landward flows in the deep Ambrose Channel (NOS03*B*). Comparisons at the Narrows (NOS17) and Hudson River (NOS36*S*) are also quite favorable, although weaker density-induced flow (NOS17) is evident in the model results.

We have also compared the model's mean circulations in Raritan Bay with sparse observations obtained by Jefferies (1962) and Abood (1972). These circulations are primarily wind driven and are similar to those given by Hires *et al.* (1984). They are not reproduced here.

d. *Comparison of energy spectra*

We compare in Fig. 6 computed and observed energy spectra at station NOS3*S* where 30-day observations are available. The figure also gives spectra of cross-shore (Fig. 6d) and alongshore (Fig. 6e) components of wind stress and of sea level (Fig. 6c) at Sandy Hook. Cross-shore direction is defined as the direction perpendicular to the SHRP transect (positive seaward), and is nearly in the direction perpendicular to the local isobath in the adjacent continental shelf region. Alongshore direction is therefore nearly parallel to the isobath in the continental shelf region.

Model energy bands at diurnal, semidiurnal and nonlinear M_4 and M_6 periods compare quite well with observations. Note that while M_4 and M_6 sea level energies are less than diurnal (K_1 and O_1 sea level energies, M_4 and M_6 energies for velocity are of the same order as, or larger than, diurnal energies for velocity. Thus nonlinear wave interactions are important. The simulated spectral shape at high frequency (period less than 12 hours) also agrees quite well with observation, as can be seen from the smoothed spectra shown in Figs. 7a, b. The model's energy spectrum in Fig. 7a follows a k_n^{-3} behavior, in agreement with two-dimensional turbulence theory (Fjortoft, 1953; Kraichnan, 1967; Leith, 1971). Here, k_n is a nondimensionalized wavenumber defined as $k_n = (\omega/U) \cdot B$, where $B = 5$ km is taken as a typical cross-sectional dimension of the estuary, ω is frequency and U is somewhat arbitrarily taken to be 0.2 m s^{-1}. The model's "k_n^{-3}" behavior at large wavenumbers suggests that the model's grid sizes are sufficiently refined to correctly resolve small-scale eddies and hence shear dispersion processes in the estuary.

e. *Subtidal response to wind forcing*

For time scales greater than one day, the dominant forcing is the wind stress manifest in two forms: directly, through local surface stress and indirectly, at open boundaries through sea level variation induced by winds over the continental shelf. Spectra of observed velocity (Fig. 6b) and sea level (Fig. 6c) show maxima at periods that correspond to maxima in spectra of wind stresses (Figs. 6d, e). Similar maxima can also be seen in the simulated velocity spectrum (Fig. 6a). For periods longer than ten days, the simulated energy is some five times less than is observed.

To study the relations between winds and simulated and observed velocities we show in Fig. 8 square coherencies and phase spectra between cross-shore ve-

TABLE 4. Comparison of simulated and observed mean currents (cm s^{-1}), positive seaward. NOS 1980 observation at 05B is not entirely reliable.

	NOS station								
	01S	03S	03B	05S	05B	17S	17M	17B	36S
Simulation	−6	9	−1	5	1.6	10	−4	−5	2
NOS 1980 observation	−14	5	−1.5	6	−3	11	−6	−8	2
Observation, from Doyle and Wilson (1978)	−3	10	<0	12.5	−6	—	—	—	—

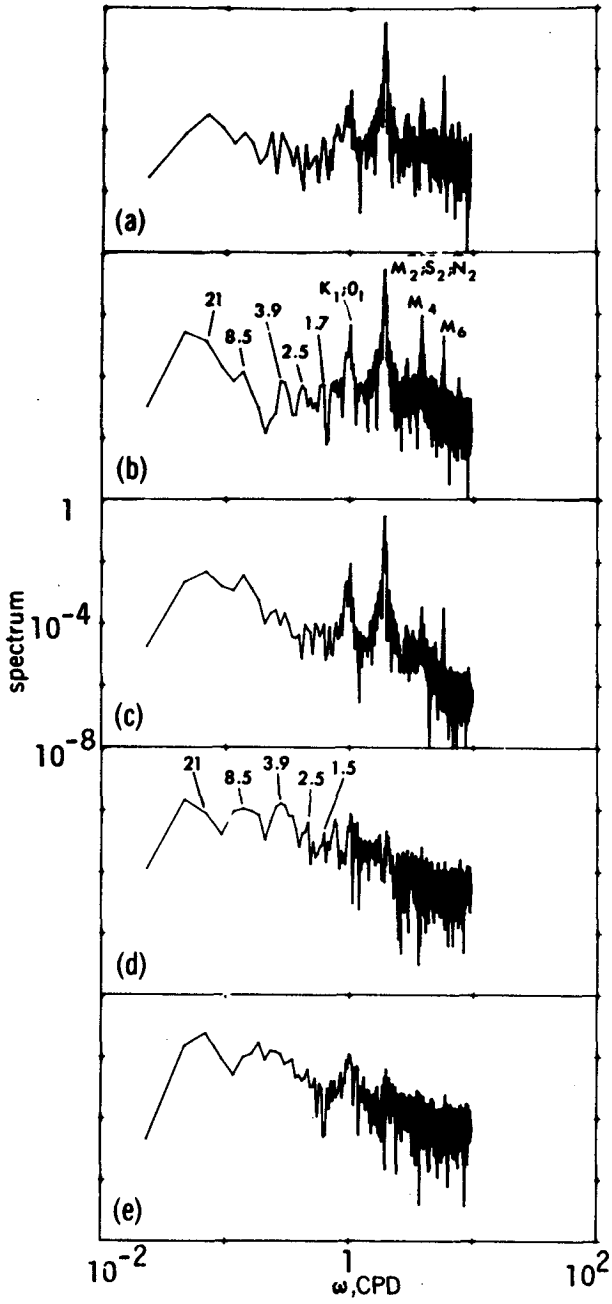

FIG. 6. Energy spectra of (a) simulated cross-shore current at NOS03*S*, (b) observed cross-shore current at NOS03*S*, (c) simulated sea level at Sandy Hook, (d) cross-shore wind and (e) alongshore wind. Numbers in (b) and (d) give periods in days.

locities at NOS03*S* and cross-shore wind stress. Simulated (cross-shore) velocity is correlated with cross-shore wind at 4.2- and 1.4-day periods (Fig. 8b), in fair agreement with observations, which show correlations at 4- and 1.3-day periods (Fig. 8a). There is also a peak around the 20-day period, but its clear interpretation is not possible with the 30-day record we have analyzed. Its phase difference of 180° does suggest a baroclinic wind response for long-period motions: increased offshore surface flow produces a corresponding increased onshore bottom flow. At shorter periods, observations show that cross-shore currents lead cross-shore winds by about 110° at the 4-day period and by about 70° at the 1.3-day period. This compares with 135° and 70°, respectively, computed by the model. Part of this phase lead response is accounted for by barotropic dynamics. Figure 9 shows plots of squared coherency and phase spectrum between cross-shore, depth-averaged velocity at NOS03 and cross-shore wind stress, which also give high coherencies around the 4- and 1.3-day periods with phase leads of 22° and 40°, respectively. In a study of nearshore (depth < 15 m) current meter observations off the South Carolina coast, Schwing *et al.* (1983) found that cross-shore currents lead cross-shelf winds by about 10 hours at 5-day period, or about 30° phase lead. This finding is consistent with ours and suggests similar governing dynamics. One can idealize NOS03 as a nearshore current meter station of the adjacent continental shelf, and consider for simplicity the following "steady state" (i.e., motion is induced by periodic winds with frequency of motion ω much less than Coriolis frequency f; for more details see Schwing *et al.*, 1985, where a more general time-dependent analysis for variable H is given) transport equations:

$$-fV = -gH\eta_x + \tau^x - rU/H$$

$$fU = \tau^y - rV/H.$$

Eliminating V, we obtain

$$[r/H + f^2/(r/H)]U = [\tau^x + f\tau^y/(r/H)] - [gH\eta_x].$$

Here, x is (cross-shore) positive seaward or approximately to the southeast; y is the alongshore axis, positive approximately to the northeast; $r = 10^{-3}$ m s^{-1} is the linear friction coefficient, and other notations are standard. The last equation shows a directly wind forced transport and a transport induced by sea level pressure gradient set up by the wind, represented respectively by the two square-bracketed terms on the right-hand side. A northwestward or southwestward (negative τ_x or τ^y) wind produces a northwestward transport. At the same time a negative cross-shore pressure gradient (sea level decreasing offshore) is produced that tends to produce a southeastward transport, opposite to the direct wind-induced transport. When winds begin blowing southeastward or northeastward (positive τ^x or τ^y), cross-shore transport is already southeastward, in response to the negative cross-shore sea level gradient, thus leading the wind in time. Schwing *et al.* (1985) show that, for low-frequency motion such that $r/H \approx f \gg \omega$, the phase lead is close to, but less than, 45°.

Barotropic dynamics alone do not give a complete picture of the response. This is especially true for NOS03*S* located some 5 m below the water surface at

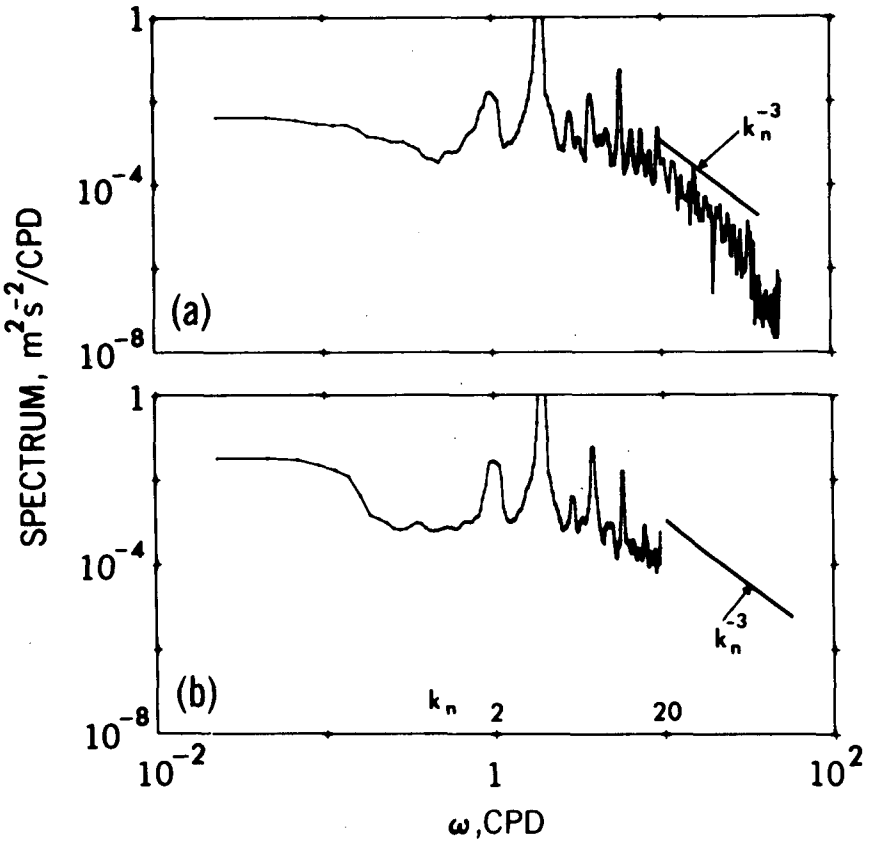

FIG. 7. Smoothed energy spectra of (a) simulated and (b) cross-shore currents at NOS03*S*.

the mouth of an estuary where local baroclinic and shearing velocity responses are important. These responses will also result in phase leads, perhaps augmenting further phase leads induced by the barotropic wind response. The phase lead of 110° at the 4-day period is likely a result of this baroclinic response. An offshore wind in this case drives a stronger density-induced two-layer circulation, with larger offshore transport of less-saline water near the surface layer, and a correspondingly larger onshore transport of ocean water in the bottom layer. Wind in the opposite direction has the opposite effect.

4. Discussions

We have compared simulation results of the Hudson–Raritan estuary with available observations. By and large, the model performed reasonably well in reproducing detailed features of velocity and salinity fields in the estuary. Observations confirm the model's prediction of the existence of density advection instabilities, produced by differential advection of the three-dimensional density field. An unstable layer of water can only exist for a short time before it is mixed throughout the water column. However, because of a continuous supply of buoyancy energy from river and/or sewage discharges, the phenomenon can persist for 1–2 hours and should therefore be detectable in a carefully designed field program. The phenomenon is important because it results in intense mixing and therefore affects horizontal dispersion of salt and other contaminants in the estuary.

Simulated tidal amplitudes and phases compare well with observations. The average (over the four tide gauge stations considered) percentage difference (the error) between simulated and observed M_2 amplitudes, for example, is 6%, while the average phase difference is about 0.6°. This is a significant improvement over the two-dimensional barotropic tidal model applied to the same region with the same horizontal grid resolution, which gives an average phase error of about 3°. We interpret this improvement as being due to a better representation of bottom friction in the three-dimensional model. Future research should examine the possibility of improved tidal prediction in the estuary with a two-dimensional model, using temporally and spatially variable bottom friction obtained from the three-dimensional model. The average (over the eight current meters) percentage difference between observed and simulated M_2 current amplitudes is 12% while the phase difference is 6°.

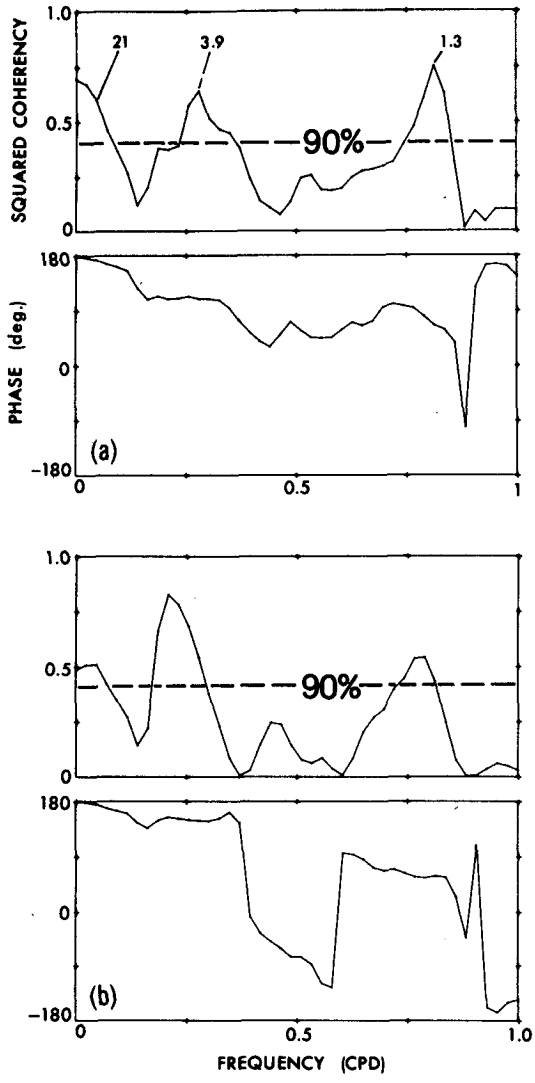

FIG. 8. Squared coherencies and phase spectra of (a) observed and (b) simulated cross-shore currents at NOS03*S* and cross-shore wind stress.

Overall temporal and spatial variations in salinities, brought about by ebbing and flooding tidal currents and large-scale eddies, and spring–neap tide effects that produce varying degrees of vertical stratification, are simulated reasonably well by the model. Discrepancies at some localized regions (near Sandy Hook and Rockaway Point, for example) can in part be explained by uncertainties in specifying exact freshwater discharges near these regions. The model also produces generally less stratification. This can be seen from a comparison of mean currents in Ambrose Channel (NOS03) and at the Narrows (NOS17) where simulated "density-induced" flows are weaker than those observed (Table 4). Smaller vertical salinity differences are also seen in the model's results during a tidal cycle (Fig. 2a, midsection), which are also a consequence of weaker density stratification and hence larger vertical mixing. We attribute this lack of stratification in the model results to neglect of temperature variation during the simulation. For example, the observed surface-to-bottom temperature difference at NOS03 averaged about 2°C. This gives a density difference that would be effectively caused by a salinity difference of about 0.6‰, which is not entirely negligible in comparison with observed and simulated salinity differences of about 2 and 1.8‰, respectively. Thus the local error in density difference can be as much as 30–40%.

We also compare simulated and observed energy spectra and study velocity responses at NOS03 to subtidal wind forcing. The model simulates reasonably well small-scale shear dispersion and gives a two-dimensional k_n^{-3} energy transfer spectrum for the nondimensionalized wavenumber k_n between 20 and 40 (or a wavelength of about 3 km). Velocity responses to subtidal winds are mixed barotropic and baroclinic responses with currents leading winds by phase angles greater than 45°. These phase leads are similar to nearshore observations made by Schwing *et al.* (1983) off the South Carolina coast, and are apparently due to a balance between frictional force, cross-shore sea surface slope and wind forcing, modified by local, vertical velocity shear and wind response to density driven flow.

5. Concluding remarks

What have we learned in our present attempt to model a real, large-scale estuary with real tidal and wind forcing and real river and sewage discharges?

1) We did not include temperature variations in the calculations. It was assumed that the large, 0–30‰ sa-

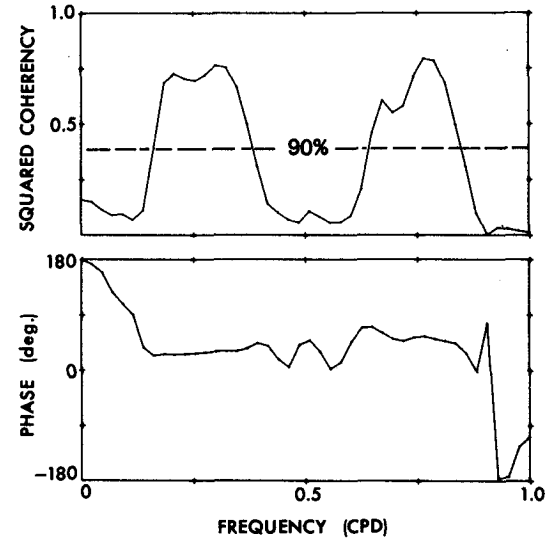

FIG. 9. Squared coherency and phase spectrum of simulated cross-shore, vertically integrated averaged current at NOS03 and cross-shore wind stress.

linity variation would dominate temperature variation in the determination of density. This is, by and large, true, except that we now recognize that the error as manifest in decreased vertical stability and increased mixing is not entirely negligible and should be avoided in future modeling efforts. This will require the inclusion of surface heat flux boundary conditions.

2) We imposed simple elevation and salinity boundary conditions at the seaward, open boundary since more detailed information was not available. An important consequence is that the dynamics are not greatly affected by this simplification.

3) For lack of more information, we assumed that wind stress could be applied, homogeneously, over the whole domain. This assumption is, by and large, reasonable, especially for the present simulation period when winds were relatively calm, and small-scale features in the estuary are predominantly topographic and tidal-induced. For periods of stronger winds, the error may be significant but can be reduced only by extensive wind data or by a limited-domain, meteorological model.

4) We have deleted horizontal diffusion terms in the momentum and salinity transport equations since these are empirical terms usually required to represent salt dispersion in an estuary and to suppress grid-scale numerical noise. Our hope that the resolution (both in horizontal and vertical directions) was sufficiently fine that small-scale, horizontal advective processes followed by vertical diffusion (the so-called Taylor dispersion processes) would correctly simulate overall horizontal dispersion seems to have been realized in most of the estuary (see also Oey *et al.*, 1985b). In narrow rivers where lateral variability is excluded, that portion of horizontal dispersion due to lateral variability is also excluded. We find, in the upper Hudson River, for example, a somewhat smaller salt intrusion than that observed. In the future, this can be improved by empirically including explicit diffusion terms in the small rivers or, better still, by resolving the small rivers laterally.

5) The most obvious error is numerical truncation error. This is most evident in the Narrows where the lateral resolution is handled by only a few grid points but differs from the lateral resolution error in the small rivers in that the Narrows is the site of large topographic variability. Increased resolution (more computer capability) or a nonrectangular numerical grid will, in the future, solve this problem.

Acknowledgments. We wish to thank Susan Salyer for preparing the manuscript. The figures were drafted by P. Tunison and processed by J. Conner. Anna Boyette and Suzanne McIntosh prepared the final version of the figures. This research was sponsored by the New Jersey Sea Grant Program under a grant from the Office of Sea Grant of NOAA, Grant 81 AA-D-0065, Project R/E-3. Additional funding was provided under Grant NA 80 RAD 00033 from the Northeast Office of the Office of Marine Pollution Assessment of NOAA. LYO was supported in part by the Visiting Scientist Program of Princeton University/NOAA, Grant 04-7-022-44017.

REFERENCES

Bedford, K. W., 1981: Spectra preservation capabilities of Great Lakes transport models. *Transport Models for Inland and Coastal Waters,* H. B. Fischer, Ed., Academic Press, 542 pp.

Bowden, K. F., L. A. Fairbairn and P. Hughes, 1959: The distribution of shearing stresses in a tidal current. *Geophys. J. Roy. Astron. Soc.,* **2,** 288–305.

Doyle, B. E., and R. E. Wilson, 1978: Lateral dynamic balance in the Sandy Hook to Rockaway Point transect. *Estuarine Coastal Mar. Sci.,* **6,** 165–174.

Duedall, I. W., H. B. O'Connors, R. E. Wilson and J. M. Parker, 1979: *The Lower Bay Complex. MESA New York Bight Atlas Monogr.,* No. 29, New York Sea Grant Inst., 47 pp.

Fjortoft, R., 1953: On the changes in the spectral distribution of kinetic energy of two-dimensional, nondivergent flow. *Tellus,* **5,** 225–230.

Hires, R. I., L.-Y. Oey and G. L. Mellor, 1984: Numerical model study of the tidal hydraulics of Raritan Bay. *Bull. N.J. Acad. Sci.,* **29,** 59–68.

Jefferies, H. P., 1962: Environmental characteristics of Raritan Bay, a polluted estuary. *Limnol. Oceanogr.,* **7,** 21–31.

Kalvaitis, A., 1982: Uncertainity estimate for oceanographic and meteorological measurements, tide and tidal current survey, New York Harbor. ESO Tech. Rep. TE3-82-002, National Ocean Survey, 38 pp.

Kraichnan, R. H., 1967: Inertial ranges in two-dimensional turbulence. *Phys. Fluid,* **10,** 1417–1423.

Leith, C. E., 1971: Atmospheric predictability and two-dimensional turbulence. *J. Atmos. Sci.,* **28,** 145–161.

Oey, L.-Y., 1984: On steady salinity distribution and circulation in partially mixed and well mixed estuaries. *J. Phys. Oceanogr.,* **14,** 629–645.

——, G. L. Mellor and R. I. Hires, 1985a: A three-dimensional simulation of the Hudson–Raritan estuary. I: Description of the model and model simulations. *J. Phys. Oceanogr.,* **15,** 1676–1692.

——, —— and ——, 1985b: A three-dimensional simulation of the Hudson–Raritan estuary. III: Salt flux analyses. *J. Phys. Oceanogr.,* **15,** 1711–1720.

——, —— and ——, 1985c: Tidal modeling of the Hudson–Raritan estuary. *Estuarine Coastal Shelf Sci.,* **20,** 511–527.

Quirk, Lawler and Matusky Engineers, 1971: Environmental effects of Bowline generating station on Hudson River. QL and M Project No. 169-1, 212 pp.

Schwing, F. B., B. Kjerfve and J. E. Sneed, 1983: Nearshore coastal currents on the South Carolina continental shelf. *J. Geophys. Res.,* **88,** 4719–4729.

——, L.-Y. Oey and J. O. Blanton, 1985: Frictional response of continental shelf water to local wind forcing: Observations and theory. *J. Phys. Oceanogr.,* **15,** 1733–1746.